HHS Public Access

Author manuscript

Cancer Res. Author manuscript; available in PMC 2021 July 01.

Published in final edited form as:

Cancer Res. 2021 January 01; 81(1): 91–102. doi:10.1158/0008-5472.CAN-20-1293.

Secretory mucin 5AC promotes neoplastic progression by augmenting KLF4-mediated pancreatic cancer cell stemness

Koelina Ganguly[1,*], **Shiv Ram Krishn**[1,*], **Satyanarayana Rachagani**[1], **Rahat Jahan**[1], **Ashu Shah**[1], **Palanisamy Nallasamy**[1], **Sanchita Rauth**[1], **Pranita Atri**[1], **Jesse L. Cox**[2], **Ramesh Pothuraju**[1], **Lynette M. Smith**[3], **Sudhua Ayala**[1], **Christopher Evans**[5], **Moorthy P. Ponnusamy**[1], **Sushil Kumar**[1], **Sukhwinder Kaur**[1,#], **Surinder K. Batra**[1,4,#]

[1]Department of Biochemistry and Molecular Biology, University of Nebraska Medical Center, Omaha, Nebraska, USA

[2]Department of Pathology and Microbiology, University of Nebraska Medical Center, Omaha, Nebraska, USA

[3]Department of Biostatistics, College of Public Health, University of Nebraska Medical Center, Omaha, Nebraska, USA

[4]Fred and Pamela Buffett Cancer Center, Eppley Institute for Research in Cancer and Allied Diseases, University of Nebraska Medical Center, Omaha, Nebraska, USA

[5]Division of Pulmonary Sciences and Critical Care Medicine, University of Colorado Denver School of Medicine, Aurora, Colorado, USA

Abstract

Secreted mucin 5AC (MUC5AC) is the most abundantly overexpressed member of the mucin family during early pancreatic intraepithelial neoplasia stage I (PanIN-I) of pancreatic cancer (PC). To comprehend the contribution of Muc5ac in PC pathology, we genetically ablated it in an autochthonous murine model (KrasG12D; Pdx-1cre, KC), which mirrors the early stages of PC development. Neoplastic onset and the PanIN lesion progression were significantly delayed in Muc5ac knockout (KrasG12D; Muc5ac−/−; Pdx-1cre, KCM) animals with a 50% reduction in PanIN-2 and 70% reduction in PanIN-3 lesions compared to KC at 50 weeks of age. High-throughput RNA-sequencing analysis from pancreatic tissues of KCM animals revealed a significant decrease in cancer stem cell (CSC) markers Aldh1a1, Klf4, EpCAM, and CD133. Further, the silencing of MUC5AC in human PC cells reduced their tumorigenic propensity, as indicated by a significant decline in tumor formation frequency by limiting dilution assay upon

[#]**To whom correspondence should be addressed**: Surinder K. Batra and Sukhwinder Kaur, Ph.D., Department of Biochemistry and Molecular Biology, Eppley Institute for Research in Cancer and Allied Diseases, University of Nebraska Medical Center, 985870 Nebraska Medical Center, Omaha, NE, 68198-5870, U.S.A., Phone: 402-559-5455; Fax: 402-559-6650, sbatra@unmc.edu; Skaur@unmc.edu.

[*]Equal Contribution

Author Contributions

KG and SRK performed the experiments and analyzed the results. KG, SRK, MPP, SKumar, SKaur, and SKB designed the research and edited the manuscript. SRachagani, RJ, AS, PN, SRauth, RP, and SA provided experimental assistance and technical support. PA helped in the analysis of RNA seq. data. LMS helped in the statistical analysis of the data. JLC helped in scoring and understanding of histologic data. CE provided Muc5ac-knockout mice. All authors contributed to reviewing and editing the manuscript.

Competing interests

SKB is one of the co-founders of Sanguine Diagnostics and Therapeutics, Inc. The other authors declare no competing interests.

subcutaneous administration. The contribution of MUC5AC in CSC maintenance was corroborated by a significant decrease in tumor burden upon orthotopic implantation of MUC5AC-depleted PC cells. Mechanistically, MUC5AC potentiated oncogenic signaling through integrin αvβ5, pSrc (Y416), and pSTAT3 (Y705). Phosphorylated STAT3, in turn, upregulated Klf4 expression, thereby enriching the self-renewing CSC population. A strong positive correlation of Muc5ac with Klf4 and pSTAT3 in the PanIN lesions of KC mouse pancreas reinforces the crucial involvement of MUC5AC in bolstering the CSC-associated tumorigenic properties of Kras-induced metaplastic cells, which leads to PC onset and progression.

Significance—The current study elucidates that de novo expression of MUC5AC promotes cancer cell stemness during Kras-driven pancreatic tumorigenesis and can be targeted for development of a novel therapeutic regimen.

Keywords

Pancreatic cancer; PanIN; MUC5AC; stemness; tumorigenesis

Introduction

Pancreatic cancer (PC) ranks as the third deadliest malignancy with a five-year survival rate of 9.3%, due to asymptomatic progression, molecular heterogeneity, and early dissemination (1). The constitutively active Kras mutation, present in 95% of the PC patients, is the major initiating event leading to the development of pancreatic intraepithelial neoplasia (PanIN). The PanIN lesions, manifested with cellular atypia and differential mucin expression, are the most common precursor lesions of PC that progress to invasive carcinoma (2). The dismal survival statistics and the aggressive nature of PC warrant the identification of molecular player(s) facilitating the progression of Kras-driven precursor lesions to invasive ductal carcinoma. The Kras activation in the pancreatic parenchyma leads to the neo-to-over expression of mucins, a hallmark of PC, which significantly contributes to PC pathobiology. Gel-forming mucin 5AC (MUC5AC), one of the top differentially expressed genes and the most abundantly expressed mucin in PC, appears *de-novo* at PanIN-1A stage (3) and continue to express in tumor tissues while remaining absent in normal pancreas (4). The MUC5AC expression correlates with disease progression and has been reported as a potential diagnostic (5) and prognostic marker (6–8) in PC.

Despite ample clinical significance, very few studies have evaluated the mechanistic contribution of MUC5AC during PC pathology. The transcription factor, GLI1, has been shown to upregulate MUC5AC expression in PC cells, which disrupts E-Cadherin/β-catenin interaction leading to nuclear accumulation of β-catenin and upregulation of tumor-associated genes (9). Further, MUC5AC has been shown to obviate TRAIL-mediated cancer cell death in a xenograft model (7). Studies have also demonstrated the role of MUC5AC in the metastatic process by increasing VEGF and matrix metalloproteinases (MMPs) expression through PI3K/Akt pathways (6). However, all these studies have utilized implanted cell lines models, which seldom recapitulate the complexities of autochthonous tumors. Therefore, we genetically ablated Muc5ac in an autochthonous murine model of PC ($Kras^{G12D}$; Pdx-1cre, KC) to evaluate its contribution to PC initiation and progression. Our study demonstrated that knockout (KO) of Muc5ac resulted in a significant delay in the

neoplastic onset and progression of PC precursor lesions, and abridged the cancer cell stemness as indicated by the decreased expression of Aldh1a1, Klf4, EpCAM, and CD133. The cancer stem cells (CSCs) represent a small percentage of cells within the tumor with a self-renewing ability that primarily contributes to cancer initiation, progression, and metastasis (10–12). Our findings further suggested that MUC5AC interacts with integrin β5 in the presence of the extracellular matrix proteins, resulting in pSTAT3-mediated upregulation of Klf4, a transcription factor involved in CSC maintenance. Integrins are heterodimeric transmembrane molecules that create specialized niches for CSCs to reside and sense micro-environmental cues for proliferation, differentiation, and migration by activating numerous downstream signaling pathways (13,14). Observations from the present study have delineated that MUC5AC primes the integrin β5/pSTAT3/Klf4 signaling axis, and thereby contributes to the pro-tumorigenic and self-renewal potency of the neoplastic cells to promote Kras-induced metaplasia and PC progression.

Materials and Methods

Generation of genetically engineered mouse models (GEMMs), KC and KCM

C57BL/6 Muc5ac$^{-/-}$ mice (15), obtained from Dr. Christopher Evans at the University of Colorado, were crossed with Pdx1-Cre and LSL-Kras^{G12D} mice to obtain the genotype Kras^{G12D}; Pdx1-Cre; Muc5ac$^{-/-}$ (KCM) in the mouse pancreas. The genotyping for Kras, Pdx-1-Cre, and Muc5ac was performed by PCR using the primer sequences listed in Supplementary Table 1. The Kras^{G12D}; Pdx1-Cre (KC) and Kras^{G12D}; Pdx1-Cre; Muc5ac$^{-/-}$ (KCM) animals (male and female), were randomized and euthanized at 10, 20, 30, 40, and 50 weeks of age (3–6 animals/group/time point) (Supplementary Figure 1A).

Histologic assessment of KC and KCM pancreas

The mouse pancreatic tissues were embedded in paraffin, cut into serial tissue sections of 5 μm thickness, and stained with hematoxylin and eosin (H&E). The H&E stained slides of all the KC and KCM animals for all time points (10–50 weeks) were histologically profiled and blindly scored by the pathologist for the overall proportion of neoplastic lesions versus the normal parenchyma retained. The lesions were further histologically scored by the pathologist according to the established criteria of PanIN grades 1–3 (16). The occurrence of each of these PanIN grades was then calculated as a percentage of the total number of neoplastic lesions for each animal.

Generation of GEMM-derived organoids

Pancreas of KC and KCM mice of 50 weeks were enzymatically digested with 0.012% (w/v) collagenase XI (Sigma) and 0.012% (w/v) dispase (GIBCO) in DMEM media containing 1% FBS (GIBCO), followed by embedding them in growth factor-reduced Matrigel (BD Biosciences). Upon establishment of the organoids in enriched medium (17), they were cultured for 5, 10, 15, and 20 days. Three independent replicates of organoid culture/ time point/ group were sectioned, and their histology was visualized using H&E staining and immunohistochemistry for Muc5ac. At the end of culture, genomic DNA was isolated from the KC and KCM organoids and genotyped for the recombination of LSL-KrasG12D locus, as explained in (16).

Xenograft studies

FG/COLO357 (Scr/ShMUC5AC) cells of >95% viability were orthotopically implanted in the pancreas of randomized immunodeficient mice (male and female), at a concentration of 5×10^5 cells/50 μl/ mouse, as per the established protocol (18) (8 animals per group). All mice were sacrificed after 50 days of implantation, and the presence of metastasis to different organs (liver, spleen, lung, mesenteric lymph nodes, and on the peritoneal wall) was determined by thorough gross inspection and histological analysis. Pancreatic tumors and organs with visible metastatic lesions were excised, weighed, measured, formalin-fixed, paraffin-embedded, and were sectioned into 5 μm thick sections. 5–6 primary tumors (randomly selected) per group were stained for MUC5AC and Ki67. The percentage of $Ki67^+$ tumor cells were blindly scored by the pathologist in both groups. Metastatic organs were stained for MUC5AC and presented as representative images. This experiment was repeated twice.

Increasing dilutions of FG-Scr and FG-Sh5AC cells (10^5,10^4,10^3, and 10^2 cells in 100 μl PBS) were subcutaneously injected on left and right flanks (3–4 flanks/ cell concentration/ group) of randomized immunocompromised mice (male and female). The tumor onset was recorded in each group, and after 35 days post-implantation, the tumors were resected, and tumor weight was measured. All the animal experiments (autochthonous murine model and xenografts) were approved by the Institutional Animal Care and Use Committee (IACUC) at the University of Nebraska Medical Center.

RNA sequencing and functional enrichment of differentially expressed genes from KC and KCM mouse pancreas

The RNA sequencing was conducted on RNA isolated from age-matched KC and KCM pancreatic tissues. The raw sequences were mapped to the mouse genome (UCSC mm10), downloaded from iGenomes using TopHat (RRID: SCR_013035). The bam files were assessed with CuffLinks (RRID: SCR_014597), and a differential gene expression profile in the KC and KCM animals were generated using CuffDiff (RRID: SCR_001647) (19). A volcano plot was made using R bioconductor (RRID:SCR_006442) to represent the differentially expressed genes (20). ConsensusPathDB (http://cpdb.molgen.mpg.de/) (RRID: SCR_002231) (21), (22) was then used to assess the gene ontology (GO) terms differentially regulated in KCM. The top hits from this pathway analysis were assessed using gene set enrichment analysis (GSEA) (23).

Statistical Analyses

The power analysis for animal numbers was performed using an alpha error probability of 0.05 and a power level of 0.8. Two-tailed independent sample student's t-test was used for comparison of normally distributed data. Non-normally distributed data were analyzed by the nonparametric Wilcoxon rank-sum test. All the *in vitro* experiments were performed independently at least three times with proper biological and technical replicates. A p-value of <0.05 was considered statistically significant.

SW1990 and FG/COLO357 cells were obtained from American Type Culture Collection (ATCC) and Dr. Ohsawa, University of Tokyo, Japan respectively. Both the cell lines used in

the study were authenticated by short tandem repeat (STR) DNA profiles as per standard guidelines every six months, were regularly confirmed to be free of *Mycoplasma* contamination, and were used at a passage number less than 10. The detailed description of *in vitro* assays, cell lines, and reagents [sequences of primers and shRNAs (Supplementary Table 1), sources of antibodies (Supplementary Table 2.1, 2.2)] used for the study are provided in the Supplementary Material and Methods.

Results

Genetic deletion of Muc5ac delays onset and progression of neoplastic lesions in the pancreas:

To explore the role of Muc5ac in PC onset and progression, the KC and KCM mice were euthanized at 10, 20, 30, 40, and 50 weeks of age; pancreases were resected, weighed, and histologically assessed for the neoplastic changes (Figure 1A). Pathological scoring revealed a greater percentage of normal parenchyma retained in KCM mice at 20 ($p<0.05$), 30 ($p<0.01$), and 50 ($p<0.05$) weeks of age, as compared to KC mice (Figure 1B). Further analysis of pancreatic tissue at 20 weeks of age revealed a significantly lower frequency of neoplastic lesions in the KCM mice in comparison to KC, suggesting a delay in PC onset.

The PanIN lesions were graded at different weeks of progression (n=3–6 animals/week/cohort). A consistent decrease in the percentage of medium (PanIN-II) and high grade (PanIN-III) lesions were observed in KCM mice during different weeks of progression. At 30 weeks, KC mice showed the development of PanIN-3 (3.3% of the pancreas) besides extensive PanIN-I (76.6% of the pancreas) and PanIN-II (11.6% of the pancreas), whereas age-matched KCM mice predominantly comprised of low grade, PanIN-I (65%) and PanIN-II (1.6%), which was apparent at 50 weeks of age, with a 50% reduction in PanIN-2 and a 70% reduction in PanIN-3 lesions in the KCM group as compared to KC (Figure 1C), suggesting that Muc5ac supports PC progression. Additionally, the average weight of the pancreas isolated from the KC animals was greater as compared to age-matched KCM mice, especially at 50 weeks of age (Supplementary Figure 1B).

Next, we generated 3D-organoids from age-matched KC and KCM mice pancreas and genotyped the same for recombination event at LSL-$Kras^{G12D}$ locus (Supplementary Figure 1C). Interestingly, a higher percentage of KCM organoids lost their viability after 15 days in culture, while the KC organoids persistently proliferated even at 20 days in culture. The quantitative assessment of organoid size showed a 50% reduction in KCM group compared to KC (Figure 1D, E), which indicates the role of Muc5ac in the sustained survival of malignant cells. Furthermore, H&E-stained sections of KC organoids demonstrated complex papillary architecture, nuclear atypia, and budding of cell clusters in the ductal lumen, resembling the histology of advanced PanIN-2 to PanIN-3 lesions, as compared to the simpler architecture of the KCM organoids, resembling the histology of early PanIN lesions (Figure 1F).

Abrogation of MUC5AC decreases stemness in the neoplastic pancreas of mouse and human PC cells:

To identify the potential downstream targets of Muc5ac in facilitating PC progression, RNA sequencing was performed on the pancreatic tissue from 50 weeks old KC and KCM animals (GSE160029). The top significantly downregulated genes were associated with CSC maintenance and epithelial-to-mesenchymal transition (EMT) (Figure 2A). The qRT-PCR validation of RNA seq analysis showed significant downregulation of Aldh1a1, Dclk1, Klf4, CD133, CD44, Zeb1, and EpCAM in KCM as compared to KC, validating the RNA-seq. analysis (Figure 2B). Immunofluorescence (IF) studies revealed a decrease in $Klf4^{+}$ ductal epithelial cells in the KCM pancreas (Figure 2C), with a strong positive correlation (R^2=0.78) of Muc5ac and Klf4 expression in the PanIN lesions of KC mouse (Figure 2D). Concurrently, there was a significant decline in Aldh1a1-positive (Supplementary Figure 1D, E), and EpCAM-positive (Supplementary Figure 1F, G) ductal cells in the PanIN lesions in KCM, as compared to the KC mice. Klf4 has been shown to induce ductal phenotype and promote PanIN progression in the presence of $Kras^{G12D}$ mutation (24,25). The strong positive correlation of Muc5ac and Klf4 in the ductal lesions, with a concomitant elevation of other CSC markers in the KC mouse, suggests that MUC5AC/Klf4 axis may be involved in the maintenance of self-renewing CSC population during murine PC progression.

Next, we asked whether the MUC5AC-mediated enrichment of cancer cell stemness exists in human PC cells. An evaluation of a panel of human PC cell lines demonstrated a high to a medium expression of MUC5AC in FG/COLO357, SW1990, and BxPC3, while telomerase-transformed normal pancreatic ductal epithelial cell line HPNE lacked MUC5AC expression (Supplementary Figure 2A). As MUC5AC is a secreted mucin, its expression was validated in culture supernatant by enzyme-linked immunosorbent assay (Supplementary Figure 2B), and IF analysis showed surface and diffused cytoplasmic staining (Supplementary Figure 2C). MUC5AC was stably silenced in two PC cell lines, FG/COLO357, and SW1990, (Supplementary Figure 2D, E, F, G) using two different shRNA sequences. The knockdown (KD) cell lines, when analyzed for CSCs by dye exclusion side population (SP) analysis, showed 87% and 55% decline in the percentage of SP cells in FG/COLO357, and SW1990 cells, respectively (Figure 2E, F). This was further corroborated by a decrease in the expression of stemness markers, Aldh1a1, Sox9, Klf4, EpCAM, CD133, and CD44 in the KD cell lines (Figure 2G).

Silencing of MUC5AC drastically reduces the tumorigenic propensity of PC cells *in vitro* and *in vivo*:

Accumulating evidence supports the role of CSCs in tumorigenesis and metastasis of PC cells (11,12). MUC5AC-silenced PC cell lines, FG/COLO357 (FG-Sh5AC) and SW1990 (SW-Sh5AC), demonstrated G1/S arrest, with a 14% ($p<0.05$) and 19% ($p<0.001$) increase in the percentage of cells in G1 phase, with a concurrent decrease of 12% and 19% of cells in the S-phase, respectively (Figure 3A, Supplementary Figure 2H). Expression of cell cycle regulators responsible for G1 to S transition like Cyclin-D1 and Cyclin-E were also downregulated upon MUC5AC silencing (Figure 3B, Supplementary Figure 2I). The MUC5AC-deficient cells formed significantly fewer colonies ($p<0.001$) in a soft agar assay, suggesting that MUC5AC assists in anchorage-independent growth of PC cells (Figure 3C).

Additionally, KD of MUC5AC moderately reduced cell viability under nutrient-deprived condition, as assessed by MTT assay under reduced serum (1%) conditions (Supplementary Figure 2J, K).

Orthotopic implantation of FG-Scr and FG-Sh5AC cells into the pancreas of nude mice showed a significant reduction ($p<0.01$) in tumor weight (Figure 3D) in FG-Sh5AC group (Mean±SE, 303±74.3 mg) as compared to FG-Scr control (Mean±SE, 801±195.5 mg). This was further supported by a distinct decrease in the percentage of proliferative $Ki67^+$ tumor cells in the MUC5AC silenced group (Figure 3E, Supplementary Figure 2L). The findings were corroborated in the autochthonous mouse model, which demonstrated a similar trend in the decline in the percentage of $Ki67^+$ ductal cells in the KCM pancreatic tumors compared to KC across all weeks of progression (Figure 3F, Supplementary Figure 2M). In order to address whether MUC5AC's ability to enhance the tumorigenic potential and proliferative index of cancer cells is dependent on the maintenance of CSCs, we performed *in vitro* and *in vivo* limiting dilution assays. FG-Sh5AC cells demonstrated a significant decline in spheroid-forming ability under low-attachment (Figure 3G, H) followed by attachment in normal plate (Figure 3I, Supplementary Figure 3A) conditions. The reduction in colony size was more evident at lower dilution of cells, which was further corroborated upon subcutaneous implantation of serially diluted FG-Scr and FG-Sh5AC cells (Figure 3J). While 1×10^3 FG-Scr cells could form detectable tumors after 35 days post-implantation, no tumor was detected with the same number of FG-Sh5AC cells (Figure 3K), suggesting that the tumor-initiating CSC population is enriched in the presence of MUC5AC. The significant decline in the tumor weight of the MUC5AC-depleted group (Figure 3L) further reinstates that MUC5AC-associated CSC maintenance provides pro-tumorigenic growth advantage to the PC cells.

Further, corroborating our RNA-seq. analysis that demonstrates the downregulation of EMT-associated genes in KCM mouse, silencing of MUC5AC reduced the migratory propensity of PC cells by 85%, as observed in transwell migration assay (Figure 4A), wound healing assay (Supplementary Figure 3B), and by phalloidin staining-based actin polymerization (Supplementary Figure 3C). Alongside, we observed a reduction in metastatic incidences to peritoneum, intestine, diaphragm, liver, lung, and mesenteric lymph nodes in the mice bearing FG-ShMUC5AC orthotopic tumors as compared to FG-Scr control (Figure 4B, Supplementary Figure 3D, E), which maintained MUC5AC expression in the metastatic lesions (Figure 4C). The gene set enrichment (GSE) analysis on the RNA seq data showed significant enrichment for the genes involved in cell migration in the KC mouse pancreatic tissue (Figure 4D), supporting the premise that MUC5AC-expressing PC cells have a higher metastatic propensity. MMP-2 and MMP-9 were among the top significantly downregulated genes in the KCM tumors. Moreover, a significant decrease in MMP-2 and MMP-9 expression was observed in the FG-Sh5AC tumor as compared to the FG-Scr group (Figure 4E). Interestingly, enhanced activity of MMP-2 and MMP-9 was observed in gelatin gel-zymography, where FG-Sh5AC cells were treated with MUC5AC-enriched conditioned media (CM) from FG-Scr cells (Figure 4F). Cumulatively, our *in vitro* and xenograft studies recapitulate the observation from the autochthonous murine model that MUC5AC potentiates CSC maintenance, which is further manifested by high tumorigenic and metastatic propensity of MUC5AC-expressing PC cells.

MUC5AC contributes to the tumorigenic potential of PC cells through integrin β5:

To identify the molecular players that are mechanistically involved in the MUC5AC-mediated pro-tumorigenic phenotype of PC cells, we performed GSEA analysis using our RNA seq. data that indicated that loss of MUC5AC significantly impacted integrin-mediated signaling in the KCM tumors (Figure 5A). Furthermore, Gene Ontology (GO)-based clustering from the RNA -seq data revealed integrin-mediated cell-adhesion (GO: 0033632 and GO: 0033628) as the top differentially regulated pathways (FDR: 0.017, 0.001) with scores 4.4 and 3.0, respectively. Thus, we evaluated the expression of multiple integrins and observed a significant loss of integrins αv and β5 in MUC5AC-KD cells compared with controls (Figure 5B). We investigated the phosphorylation of Src, a mediator of integrin signaling, and observed that KD of MUC5AC reduced Src phosphorylation at tyrosine 416 (Y416) (26) compared to control cells (Figure 5B). Downstream of activated Src cascade, MUC5AC silencing significantly reduced the phosphorylation of STAT3 at tyrosine 705 (Y705) compared to scramble controls (Figure 5B). Quantitatively, there was a significant and consistent decline in integrin β5, pSrc, and pSTAT3 levels upon MUC5AC ablation (Figure 5C). To address whether MUC5AC, a secreted gel-forming molecule, devoid of any known putative signaling domain, can enhance the tumorigenicity of PC cells through integrin αvβ5/Src/STAT3 axis, FG-Sh5AC cells were treated with conditioned media from FG-Scr cells, which substantially rescued integrin β5 expression in FG-Sh5AC cells (Figure 5D, E). Interestingly, MUC5AC co-immunoprecipitated integrin β5 on fibronectin-coated plates (Figure 5F), suggesting that integrin αvβ5 may undergo a conformational change upon interaction with its ligand (fibronectin), which facilitates its interaction with MUC5AC. Additionally, FG-Sh5AC cells, which demonstrated a significantly reduced attachment and proliferation on fibronectin and vitronectin-coated plates, key ligands for integrins αv and β5, showed a drastic increase in attachment (Supplementary Figure 3F) and proliferation (Figure 5G) upon treatment with the FG-Scr media, almost comparable to that of Scr control. Furthermore, the transient KD of integrin β5 significantly impaired the migratory potential of MUC5AC-expressing PC cells, almost to the extent seen in MUC5AC-silenced cells. The combined loss of MUC5AC and integrin β5 completely abrogated motility of the PC cells (Figure 5H, Supplementary Figure 3G). Immunohistochemical analysis of human PC tissues for MUC5AC and integrin αvβ5 showed their spatial co-expression in PanINs as well as in well-differentiated and poorly differentiated tumors (Figure 5I), indicating a clinical relevance of this novel signaling axis. Owing to the difficulty in locating epithelial cells in the poorly differentiated tumor tissues, we focused on the PanINs and well-differentiated tumors for the quantitative analysis that suggests a strong positive correlation of MUC5AC and integrin αvβ5 expression (Figure 5J).

MUC5AC/integrin β5/pSTAT3 axis upregulates KLF4 expression to maintain PC stemness:

To address whether MUC5AC/Integrin β5-mediated signaling cascade, through pSrc-Tyr 416 and pSTAT3-Tyr 705, regulates the stemness in PC cells, we transiently knocked down integrin β5 in MUC5AC-expressing and KD cells. The KD of integrin β5 in FG-Scr cells downregulated the phosphorylation of Src (Tyr 416) and STAT3 (Tyr 705), while the total Src and STAT3 levels remained unchanged (Figure 6A). Further supporting our proposed mechanism, pSTAT3 expression was substantially less in the KCM pancreatic tumor tissues as compared to the KC animals (Figure 6B), with a strong positive correlation ($R^2 = 0.82$) of

MUC5AC and pSTAT3 expression in the KC mouse (Figure 6C). Interestingly, neoplastic cells that abundantly expressed MUC5AC were positive for pSTAT3 expression in their nuclei (white arrowhead, Figure 6B), while cells with low MUC5AC showed lesser expression of pSTAT3 (white arrow, Figure 6B). Next, treatment of FG-Scr and FG-Sh5AC cells with C-1889, a pharmacologic inhibitor of phosphorylation and dimerization of STAT3 (27), resulted in reduced Klf4 expression (Figure 6D, E). The C1889 treatment also significantly decreased the migratory propensity of MUC5AC expressing cells (Supplementary Figure 3H). Furthermore, we observed a strong positive correlation of MUC5AC expression with that of pSTAT3 (R^2= 0.78) and Klf4 (R^2= 0.75) in the orthotopic tumor tissues (Figure 6F, G), further supporting the findings from biochemical experiments and autochthonous mouse model. To understand whether the MUC5AC-mediated CSC enrichment in PC is dependent on Klf4, we transiently knocked down Klf4 in FG-Scr and FG-Sh5AC cells and analyzed the expression of CSC markers and the percentage of SP population. Upon Klf4 KD, there was a decrease in the expression of Aldh1a1 (Figure 6H), with a concomitant decline in SP in FG-Scr and FG-Sh5AC by 95% and 60% respectively (Figure 6I, Supplementary Figure 3I). Furthermore, upon treatment with conditioned media from FG-Scr cells for 48 hours, there was an upregulation of Klf4 and Aldh1a1 in the FG-Sh5AC cells (Figure 6H) with a drastic increase in the SP (Figure 6I). However, the ablation of Klf4 in FG-Sh5AC cells blunted its response to the conditioned media treatment, as evidenced by a relatively marginal increase in SP and a moderate increase in Aldh1a1 expression.

Discussion

The constitutive activation of Kras in PC has been shown to rewire the signaling pathways leading to the expression of mucins, a hallmark of PC (28). The predominant mucins upregulated in PC include MUC1, MUC4, MUC16, and MUC5AC. Among these, MUC5AC, the most overexpressed mucin, appears *de-novo* in the early neoplastic stage (PanIN-I). In multiple malignancies, overexpression of MUC5AC has been correlated with disease progression and poor prognosis (8). Recently, survival analysis on 176 PC patients revealed that MUC5AC expression is significantly correlated to poor survival (www.proteinatlas.org). In our study, we aimed to delineate the oncogenic functions and underlying molecular mechanism of MUC5AC during the early stages of PC using a novel mouse model with genetic ablation of Muc5ac ($Muc5ac^{-/-}$) in the presence of oncogenic $Kras^{G12D}$ expression ($Kras^{G12D}$; Pdx1-Cre). Loss of Muc5ac (KCM) delayed neoplastic onset and progression of low-grade to high-grade PanINs with a significant decline in ductal proliferation as compared to KC mice. Guided by the RNA seq. analysis, which demonstrated a significant downregulation of several CSC-associated genes in KCM, and the findings from the xenograft and biochemical studies with human PC cells, we postulated that depletion of MUC5AC reduces the self-renewal propensity or cancer cell stemness, and thereby delays the neoplastic onset and disease progression in KCM. Accumulating evidence suggests the critical role of CSCs in tumor initiation and long-term clonal repopulation in many malignancies (12,29–31). Apart from the tumorigenic potential, CSCs promote EMT and impart a metastatic phenotype to the tumor (32). Interestingly, from RNA-seq analysis, multiple EMT-associated genes were significantly downregulated in KCM. This was further

corroborated by our xenograft study, which demonstrated a substantial decline in metastasis in MUC5AC-depleted group.

The GSE analysis on the RNA seq data suggested a disruption of integrin-mediated signaling in KCM, which was further corroborated in human PC cells upon MUC5AC depletion. The expression of integrin β5 was reinforced in the MUC5AC-knockdown cells by ectopic treatment of MUC5AC-enriched culture supernatant. Integrins are cellular mechanosensors that can engage with ECM components to sense micro-environmental cues, and thereby facilitate neoplastic cell growth, self-renewal, and motility by sustaining cancer stemness (13,14). A perpetual deposition of dense ECM components by activated fibroblasts, cumulatively termed as fibrosis, is a hallmark of PC (33). ECM-induced tissue stiffness promotes tumor aggressiveness via integrin-associated mechanosignaling in the epithelial cells (34). It has been previously reported that bulky glycoproteins on the tumor glycocalyx mechanically cluster integrins into adhesion plaques to augment oncogenic attributes of tumor cells (35). Among the other putative downstream pathways of integrin activation, STAT3 gets phosphorylated, which upregulates genes involved in cancer progression (36). Alongside, the chronic inflammation associated with $Kras^{G12D}$–induced tumorigenesis, activates STAT3 to sustain oncogenic growth signals, and support the early events of lung and pancreatic tumorigenesis (37), (38). A recent study precisely demonstrated a positive feed-forward loop wherein activated STAT3 in the tumor epithelial cells enhances stiff fibrotic deposition, which in turn intensifies integrin-mediated mechanosignaling to promote tumor progression (39). Furthermore, the leukemia inhibitory factor (LIF)/ STAT3 axis promotes embryonic stem cell renewal by activating Klf4 transcription (40). Klf4 was previously shown to promote the onset and progression of PanINs in the presence of $Kras^{G12D}$ mutation, by upregulating early response genes and driving acinar to ductal reprogramming (24,25). In the same context, STAT3 is essential to maintain the epithelial identity of neoplastic cells in the PanINs (37). Hence, we questioned whether MUC5AC-mediated maintenance of self-renewing CSC population during early events of $Kras^{G12D}$-driven PC is dependent on integrin β5/STAT3/Klf4 axis. Knockdown of integrin β5 suppressed phosphorylation of STAT3 at Tyr705 residue and inhibition of STAT3 phosphorylation led to diminished expression of Klf4 in the MUC5AC-expressing PC cells. Furthermore, abrogating Klf4 expression drastically reduced the stemness property of MUC5AC-expressing cells. Lastly, the strong positive correlation of Muc5ac with KLF4 and pSTAT3 in the metaplastic cells, with a concomitant enrichment of CSC markers and efficient PanIN progression in the KC mouse, suggests that MUC5AC-expressing neoplastic cells experience an advantageous self-renewal-dependent growth potency over the non-expressing cells via STAT3/Klf4 axis. Cumulatively, this study demonstrates that upon activation of oncogenic Kras, *denovo* expressed MUC5AC amplifies integrin β5/pSrc/ pSTAT3 signaling, which maintains Klf4-associated stemness or self-renewal propensity of neoplastic cells, thereby promoting Kras-induced metaplastic growth and hence culminating towards a faster PC progression (Figure 6J). Future studies will be directed to elucidate the contribution of MUC5AC in the modulation of the tumor microenvironment and paracrine mechanisms during PC progression.

Supplementary Material

Refer to Web version on PubMed Central for supplementary material.

Acknowledgements

We greatly appreciate the kind technical help of Ms. Kavita Mallya, UNMC. We also thank Dr. Jessica Mercer for her editorial contributions.

Funding: The authors/work on this manuscript were supported, in parts, by grants from the NIH (R01 CA247471, RO1 CA210637, RO1CA206444, RO1 CA183459, UO1 CA200466, PO1 CA217798, R44 CA224619, R41 CA213718, and R41 CA235984).

References

1. Rahib L, Smith BD, Aizenberg R, Rosenzweig AB, Fleshman JM, Matrisian LM. Projecting cancer incidence and deaths to 2030: the unexpected burden of thyroid, liver, and pancreas cancers in the United States. Cancer research 2014;74:2913–21 [PubMed: 24840647]
2. Distler M, Aust D, Weitz J, Pilarsky C, Grützmann R. Precursor lesions for sporadic pancreatic cancer: PanIN, IPMN, and MCN. BioMed research international 2014;2014
3. Suh H, Pillai K, Morris DL. Mucins in pancreatic cancer: biological role, implications in carcinogenesis and applications in diagnosis and therapy. American journal of cancer research 2017;7:1372–83 [PubMed: 28670497]
4. Kim GE, Bae HI, Park HU, Kuan SF, Crawley SC, Ho JJ, et al. Aberrant expression of MUC5AC and MUC6 gastric mucins and sialyl Tn antigen in intraepithelial neoplasms of the pancreas. Gastroenterology 2002;123:1052–60 [PubMed: 12360467]
5. Kaur S, Smith LM, Patel A, Menning M, Watley DC, Malik SS, et al. A Combination of MUC5AC and CA19–9 Improves the Diagnosis of Pancreatic Cancer: A Multicenter Study. The American journal of gastroenterology 2017;112:172–83 [PubMed: 27845339]
6. Yamazoe S, Tanaka H, Sawada T, Amano R, Yamada N, Ohira M, et al. RNA interference suppression of mucin 5AC (MUC5AC) reduces the adhesive and invasive capacity of human pancreatic cancer cells. Journal of Experimental & Clinical Cancer Research 2010;29:53 [PubMed: 20492722]
7. Hoshi H, Sawada T, Uchida M, Iijima H, Kimura K, Hirakawa K, et al. MUC5AC protects pancreatic cancer cells from TRAIL-induced death pathways. International journal of oncology 2013;42:887–93 [PubMed: 23292004]
8. Krishn SR, Ganguly K, Kaur S, Batra SK. Ramifications of secreted mucin MUC5AC in malignant journey: a holistic view. Carcinogenesis 2018;39:633–51 [PubMed: 29415129]
9. Inaguma S, Kasai K, Ikeda H. GLI1 facilitates the migration and invasion of pancreatic cancer cells through MUC5AC-mediated attenuation of E-cadherin. Oncogene 2011;30:714–23 [PubMed: 20972463]
10. Lee CJ, Dosch J, Simeone DM. Pancreatic cancer stem cells. Journal of clinical oncology 2008;26:2806–12 [PubMed: 18539958]
11. Sergeant G, Vankelecom H, Gremeaux L, Topal B. Role of cancer stem cells in pancreatic ductal adenocarcinoma. Nature reviews Clinical oncology 2009;6:580
12. Hermann PC, Huber SL, Herrler T, Aicher A, Ellwart JW, Guba M, et al. Distinct populations of cancer stem cells determine tumor growth and metastatic activity in human pancreatic cancer. Cell stem cell 2007;1:313–23 [PubMed: 18371365]
13. Guo W, Giancotti FG. Integrin signalling during tumour progression. Nature reviews Molecular cell biology 2004;5:816–26 [PubMed: 15459662]
14. Cooper J, Giancotti FG. Integrin signaling in cancer: mechanotransduction, stemness, epithelial plasticity, and therapeutic resistance. Cancer cell 2019;35:347–67 [PubMed: 30889378]

15. Hasnain SZ, Evans CM, Roy M, Gallagher AL, Kindrachuk KN, Barron L, et al. Muc5ac: a critical component mediating the rejection of enteric nematodes. The Journal of experimental medicine 2011;208:893–900 [PubMed: 21502330]
16. Hingorani SR, Petricoin III EF, Maitra A, Rajapakse V, King C, Jacobetz MA, et al. Preinvasive and invasive ductal pancreatic cancer and its early detection in the mouse. Cancer cell 2003;4:437–50 [PubMed: 14706336]
17. Boj SF, Hwang CI, Baker LA, Chio II, Engle DD, Corbo V, et al. Organoid models of human and mouse ductal pancreatic cancer. Cell 2015;160:324–38 [PubMed: 25557080]
18. Qiu W, Su GH. Development of orthotopic pancreatic tumor mouse models. Pancreatic Cancer: Springer; 2013. p 215–23.
19. Trapnell C, Roberts A, Goff L, Pertea G, Kim D, Kelley DR, et al. Differential gene and transcript expression analysis of RNA-seq experiments with TopHat and Cufflinks. Nature protocols 2012;7:562–78 [PubMed: 22383036]
20. Dean CB, Nielsen JD. Generalized linear mixed models: a review and some extensions. Lifetime data analysis 2007;13:497–512 [PubMed: 18000755]
21. Kamburov A, Pentchev K, Galicka H, Wierling C, Lehrach H, Herwig R. ConsensusPathDB: toward a more complete picture of cell biology. Nucleic acids research 2011;39:D712–7 [PubMed: 21071422]
22. Kamburov A, Wierling C, Lehrach H, Herwig R. ConsensusPathDB--a database for integrating human functional interaction networks. Nucleic acids research 2009;37:D623–8 [PubMed: 18940869]
23. Subramanian A, Tamayo P, Mootha VK, Mukherjee S, Ebert BL, Gillette MA, et al. Gene set enrichment analysis: a knowledge-based approach for interpreting genome-wide expression profiles. Proceedings of the National Academy of Sciences of the United States of America 2005;102:15545–50 [PubMed: 16199517]
24. Wei D, Wang L, Yan Y, Jia Z, Gagea M, Li Z, et al. KLF4 is essential for induction of cellular identity change and acinar-to-ductal reprogramming during early pancreatic carcinogenesis. Cancer cell 2016;29:324–38 [PubMed: 26977883]
25. Maddipati R, Katz JP. KLF4 initiates acinar cell reprogramming and is essential for the early stages of pancreatic carcinogenesis. Cancer cell 2016;29:247–8 [PubMed: 26977875]
26. Canel M, Serrels A, Miller D, Timpson P, Serrels B, Frame MC, et al. Quantitative in vivo imaging of the effects of inhibiting integrin signaling via Src and FAK on cancer cell movement: effects on E-cadherin dynamics. Cancer research 2010;70:9413–22 [PubMed: 21045155]
27. Redell MS, Ruiz MJ, Alonzo TA, Gerbing RB, Tweardy DJ. Stat3 signaling in acute myeloid leukemia: ligand-dependent and -independent activation and induction of apoptosis by a novel small-molecule Stat3 inhibitor. Blood 2011;117:5701–9 [PubMed: 21447830]
28. Rachagani S, Torres MP, Kumar S, Haridas D, Baine M, Macha MA, et al. Mucin (Muc) expression during pancreatic cancer progression in spontaneous mouse model: potential implications for diagnosis and therapy. Journal of hematology & oncology 2012;5:68 [PubMed: 23102107]
29. Al-Hajj M, Wicha MS, Benito-Hernandez A, Morrison SJ, Clarke MF. Prospective identification of tumorigenic breast cancer cells. Proceedings of the National Academy of Sciences 2003;100:3983–8
30. Singh SK, Hawkins C, Clarke ID, Squire JA, Bayani J, Hide T, et al. Identification of human brain tumour initiating cells. nature 2004;432:396–401 [PubMed: 15549107]
31. Boumahdi S, Driessens G, Lapouge G, Rorive S, Nassar D, Le Mercier M, et al. SOX2 controls tumour initiation and cancer stem-cell functions in squamous-cell carcinoma. Nature 2014;511:246–50 [PubMed: 24909994]
32. Scheel C, Weinberg RA. Cancer stem cells and epithelial–mesenchymal transition: concepts and molecular links. 2012. Elsevier. p 396–403.
33. Feig C, Gopinathan A, Neesse A, Chan DS, Cook N, Tuveson DA. The pancreas cancer microenvironment. AACR; 2012.
34. Vennin C, Murphy KJ, Morton JP, Cox TR, Pajic M, Timpson P. Reshaping the tumor stroma for treatment of pancreatic cancer. Gastroenterology 2018;154:820–38 [PubMed: 29287624]

35. Paszek MJ, DuFort CC, Rossier O, Bainer R, Mouw JK, Godula K, et al. The cancer glycocalyx mechanically primes integrin-mediated growth and survival. Nature 2014;511:319 [PubMed: 25030168]

36. Fofaria NM, Srivastava SK. STAT3 induces anoikis resistance, promotes cell invasion and metastatic potential in pancreatic cancer cells. Carcinogenesis 2014;36:142–50 [PubMed: 25411359]

37. D'Amico S, Shi J, Martin BL, Crawford HC, Petrenko O, Reich NC. STAT3 is a master regulator of epithelial identity and KRAS-driven tumorigenesis. Genes & development 2018;32:1175–87 [PubMed: 30135074]

38. Baratta MG. STAT3's true colours. Nature Reviews Cancer 2018;18:664–5 [PubMed: 30242216]

39. Laklai H, Miroshnikova YA, Pickup MW, Collisson EA, Kim GE, Barrett AS, et al. Genotype tunes pancreatic ductal adenocarcinoma tissue tension to induce matricellular fibrosis and tumor progression. Nature medicine 2016;22:497–505

40. Hall J, Guo G, Wray J, Eyres I, Nichols J, Grotewold L, et al. Oct4 and LIF/Stat3 additively induce Krüppel factors to sustain embryonic stem cell self-renewal. Cell stem cell 2009;5:597–609 [PubMed: 19951688]

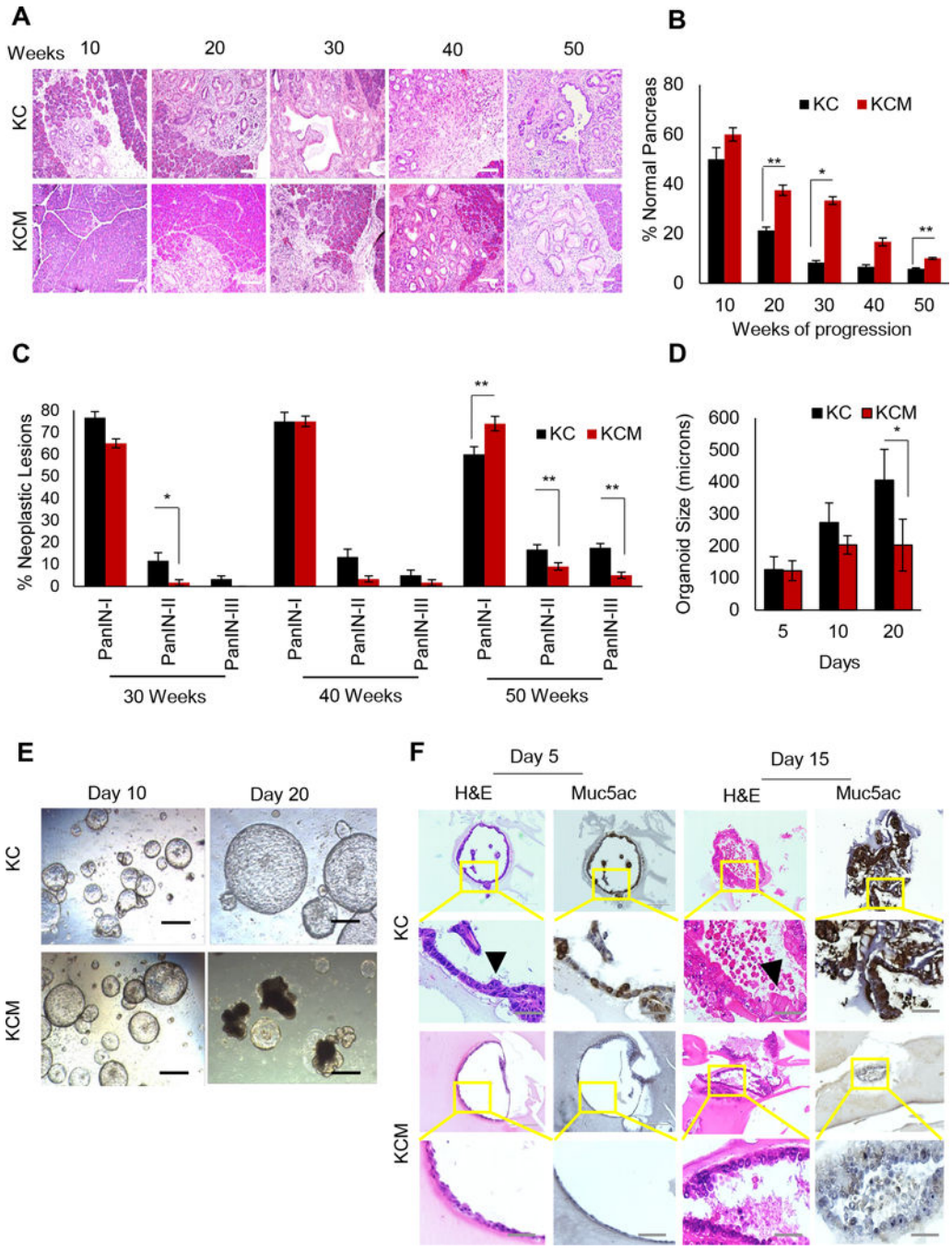

Figure 1: Genetic ablation of Muc5ac delays onset and progression of PC in the mouse model.

(A) H&E images demonstrating areas covered by precursor lesions and normal pancreas in the KC (top panel) and KCM (bottom panel) animals at indicated weeks of pancreatic cancer progression (10, 20, 30, 40 and 50 weeks of age). Scale bars, 200uM. **(B)** Quantitative analysis of pancreatic histology reveals that the pancreas of KCM animals had a significantly higher percentage of the normal pancreas as compared to the KC animals at indicated time points. **(C)** A bar graph shows the overall percentage of low and high-grade PanIN lesions from 30–50 weeks in the KC and KCM animals **(D)** Quantitative

representation of sizes (in terms of diameter) of KC and KCM organoids at Days 5, 10 and 20 of culture. **(E)** Light microscope images of KC and KCM organoids on Day 10 and Day 20 of culture. Scale bars, 400uM **(F)** H&E and immunohistochemistry of organoid sections demonstrate invasive projections and nuclear atypia in KC organoids at Day 5 of culture (black arrowhead), while the nuclear arrangement looks comparatively normal in organoids derived from KCM mice pancreas. Complex papillary structures with goblet cell-like Muc5ac-expressing morphology were evident in the KC organoids on Day 15 (black arrowhead). The KCM organoids demonstrated less advanced architecture with more organized epithelia and uniform nuclear arrangement. Scale bars, 400uM; magnified images, 200uM. (*$p<0.05$; **$p<0.005$).

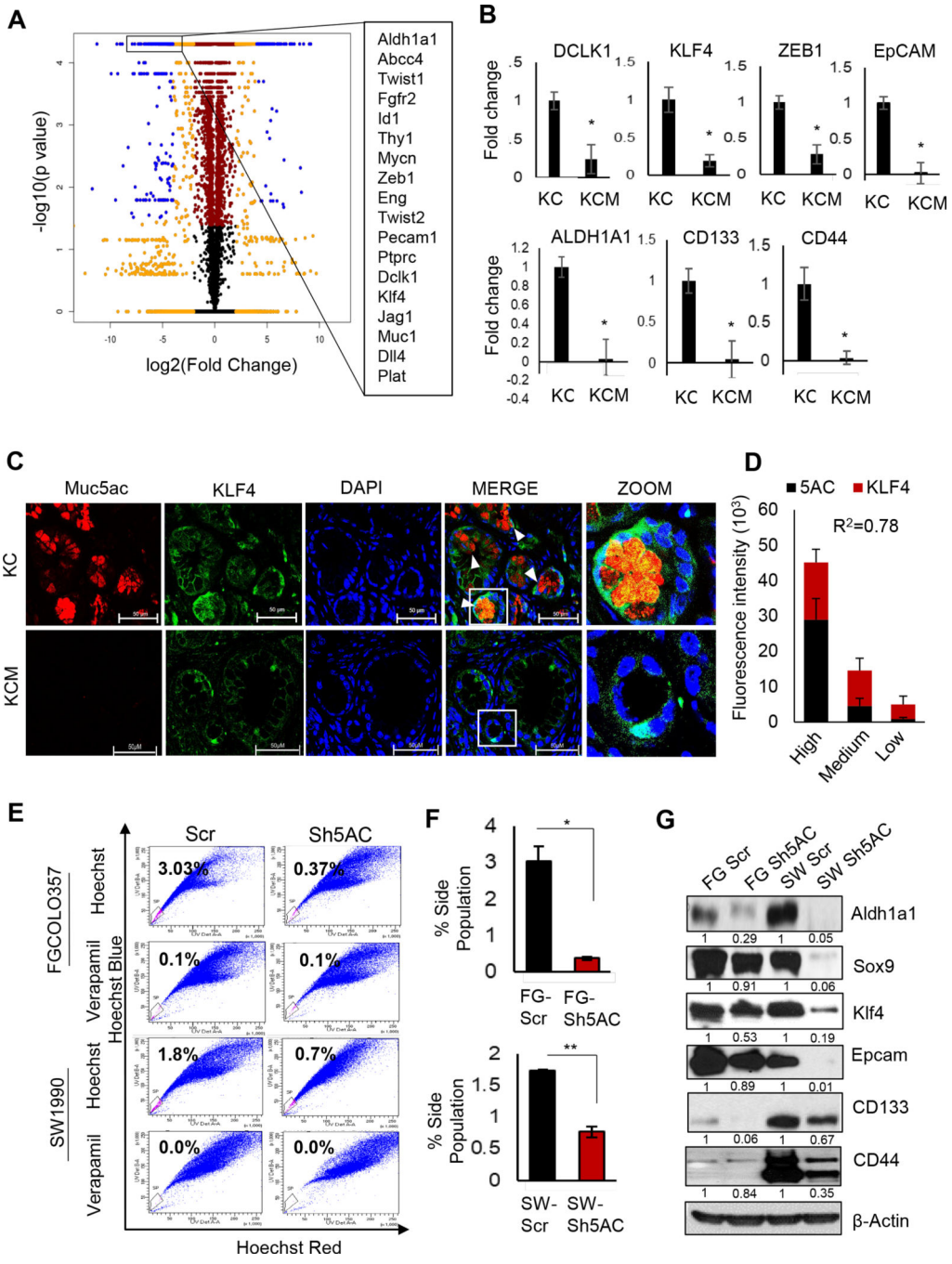

Figure 2: Depletion of MUC5AC reduces cancer stem cell (CSC) markers in the PC mouse model and human PC cells

(A) Volcano plot illustrating differentially regulated genes in the Muc5ac-knockout (KCM) animals in comparison to KC animals. Each dot represents the log2 fold change (X-axis) and the significance (p value) of the upregulation or downregulation (Y-axis) of a single gene in the KCM group. The box shows CSC genes among the top significantly downregulated genes in the KCM group. **(B)** Quantitative RT-PCR analysis was performed on the RNA isolated from the mouse pancreas showing downregulated CSC genes in KCM animals. **(C)**

Representative image from immunofluorescence analysis demonstrated a decrease in Klf4 expression in KCM as compared to KC mice (n=3–5 fields/ tissue, 3 animals). White arrowheads demonstrate areas of co-expression of Muc5ac and Klf4 in the ductal lesions. Scale bars, 50 uM. **(D)** Upon segregating the ductal epithelial cells on the basis of high, medium, and low expression of Muc5ac, there was a strong positive correlation (R^2= 0.78) of Muc5ac expression with that of Klf4 in KC mice. **(E)** Representative images from side population (SP) analysis in FG-COLO357 and SW1990 cells. **(F)** Quantitative representation of percentage SP in both the cell lines upon MUC5AC knockdown (KD). **(G)** Immunoblot showing a decrease in CSC markers after MUC5AC KD in PC cells. Relative fold change of expression of each protein (compared with respect to the control group) is mentioned under each blot (β-actin was used as a loading control for normalization).

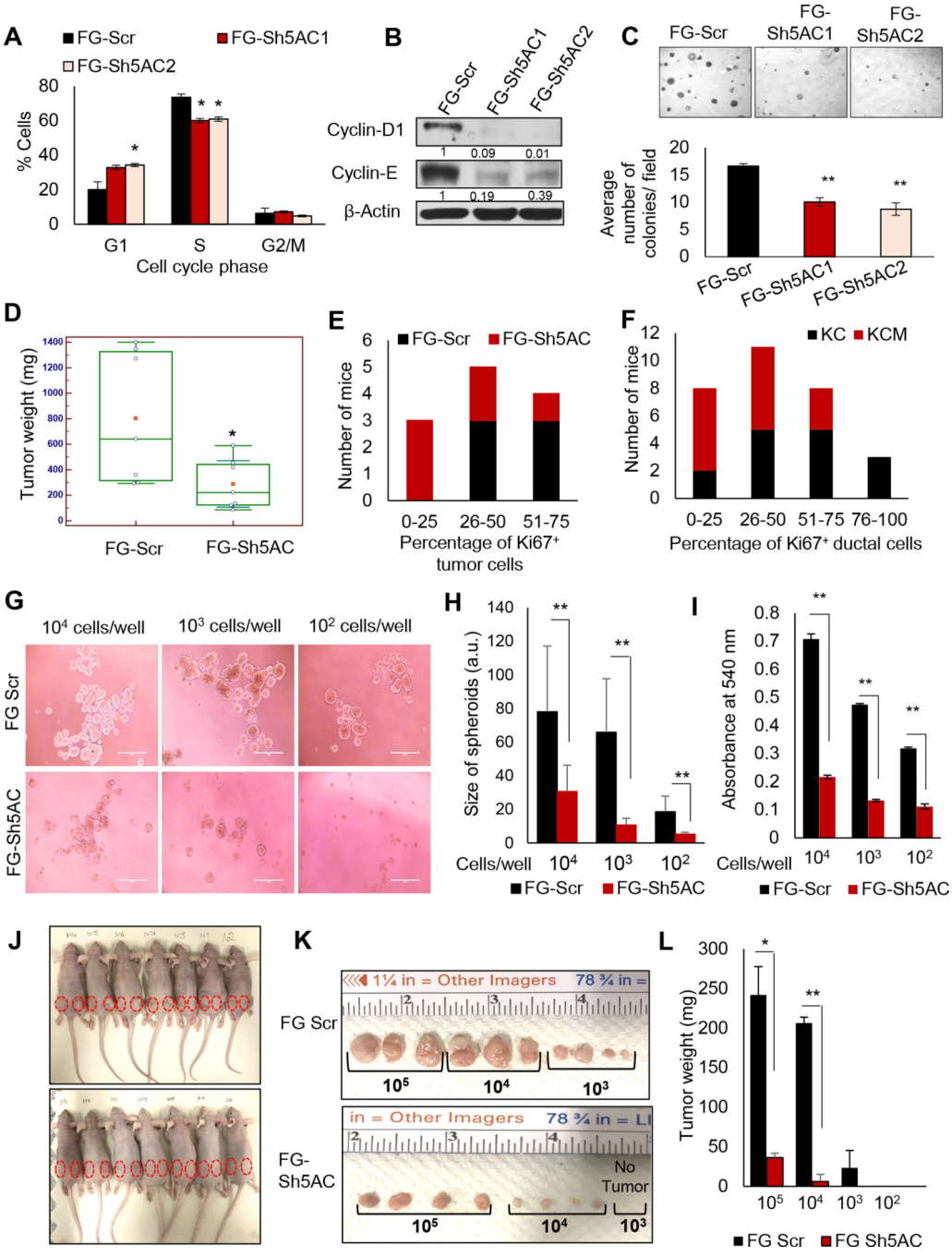

Figure 3: Loss of Muc5ac leads to the impaired tumorigenic potential of neoplastic cells.

(A) Quantitative representation of the cell cycle analysis reveals G1 to S phase arrest in FG-Sh5AC cells. **(B)** Immunoblot shows a significant reduction in Cyclins D1 and E, the key cyclins controlling G1 to S transition, upon MUC5AC KD in FG/COLO357 cells. Relative fold change of expression of each protein (compared with respect to the control group) is mentioned under each blot (β-actin was used as a loading control for normalization). **(C)** Pictorial and quantitative representations of soft-agar assay showing a significant reduction in anchorage-independent colony formation upon knockdown of MUC5AC in FG/COLO357

cells. **(D)** Box plot (N=8) showing the distribution of the tumor weight (mg) from mice orthotopically injected with FG/COLO357 MUC5AC KD (FG-Sh5AC) and scramble-control (FG-Scr) cells. Error bars represent SE for n=8 mice in each group. **(E)** Immunohistochemistry of Ki67 in FG-Scr and FG-Sh5AC-implanted pancreatic tumor sections from 6 mice/ group demonstrated a reduced percentage of $Ki67^+$ tumor cells in FG-Sh5AC mice as compared to FG-Scr group. **(F)** Reduction in the percentage of $Ki67^+$ ductal epithelial cells were observed in the KCM animals in comparison with the KC animals along with disease progression (n=15 mice/ cohort). **(G)** Representative pictures and **(H)** quantitative analysis of *in vitro* limiting dilution assay demonstrating a significant decline in the spheroids-forming propensity of MUC5AC KD cells in low attachment plate. Scale bar, 1000 uM. **(I)** Subsequent culturing of the spheroids in high attachment plate for 48 hours, followed by crystal violet staining and solubilizing the same with DMSO, demonstrates a significant decline in the colony-forming ability of MUC5AC KD cells. **(J)** Subcutaneous implantation of both flanks of athymic mice with decreasing concentrations of FG-Scr and FG-Sh5AC, viz. 10^5, 10^4, 10^3,and 10^2 cells/ flank of each mouse. **(K)** The gross examination demonstrated a drastic reduction in tumor size in all the dilutions of FG-Sh5AC cells as compared to the FG-Scr group of the same cell concentration. Unlike the FG-Scr group, no tumor was observed upon implantation of 10^3 cells in the FG-Sh5AC group. **(L)** Statistical representation of tumor weights (n= 3–4 tumors/ cell concentration/ group) in FG-Scr and FG-Sh5AC group. (*$p<0.05$; **$p<0.005$).

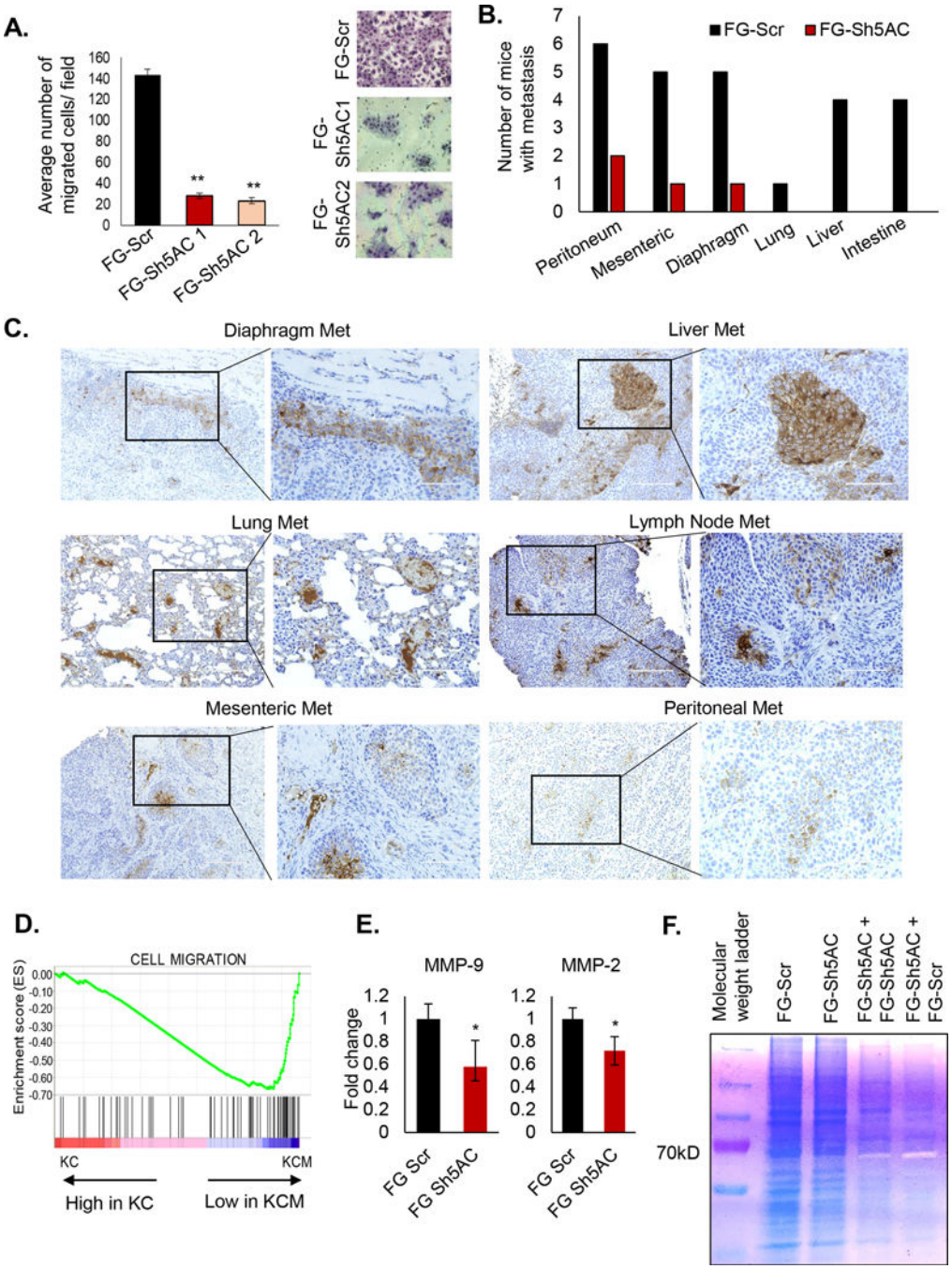

Figure 4: Loss of Muc5ac suppresses the metastatic propensity of PC cells *in vitro* and *in vivo*.

(A) Quantitative and pictorial representation of migrated FG-Scr and FG-Sh5AC cells in the Boyden-chamber assay. **(B)** The bar graph showing the number of mice having metastatic lesions in the respective organs. Incidences of metastasis were lesser in mice injected with FG-Sh5AC cells. **(C)** Immunohistochemistry showing expression of MUC5AC in metastatic lesions of liver, lung, diaphragm, and peritoneum. Scale bar, 200 uM; magnified images,100 uM. **(D)** GSEA analysis was performed on the RNA-seq. analysis from KC and KCM pancreatic tissues showing enrichment of cell migration-associated genes in KC mice and

significant downregulation of the same in the KCM group. **(E)** Quantitative PCR demonstrating a decrease in MMP-2 and MMP-9 expression in the xenograft tumors from FG-Scr and FG-Sh5AC cells. **(F)** Gelatin gel zymography showing higher proteolytic activity (clear white band in Coomassie Blue-stained background) in FG-Sh5AC cells treated with conditioned media from FG-Scr cells; the extent of proteolytic activity was lower in FG-Sh cells treated with conditioned media from FG-Sh cells, and minimal in untreated FG-Scr and FG-Sh cells. (*$p<0.05$).

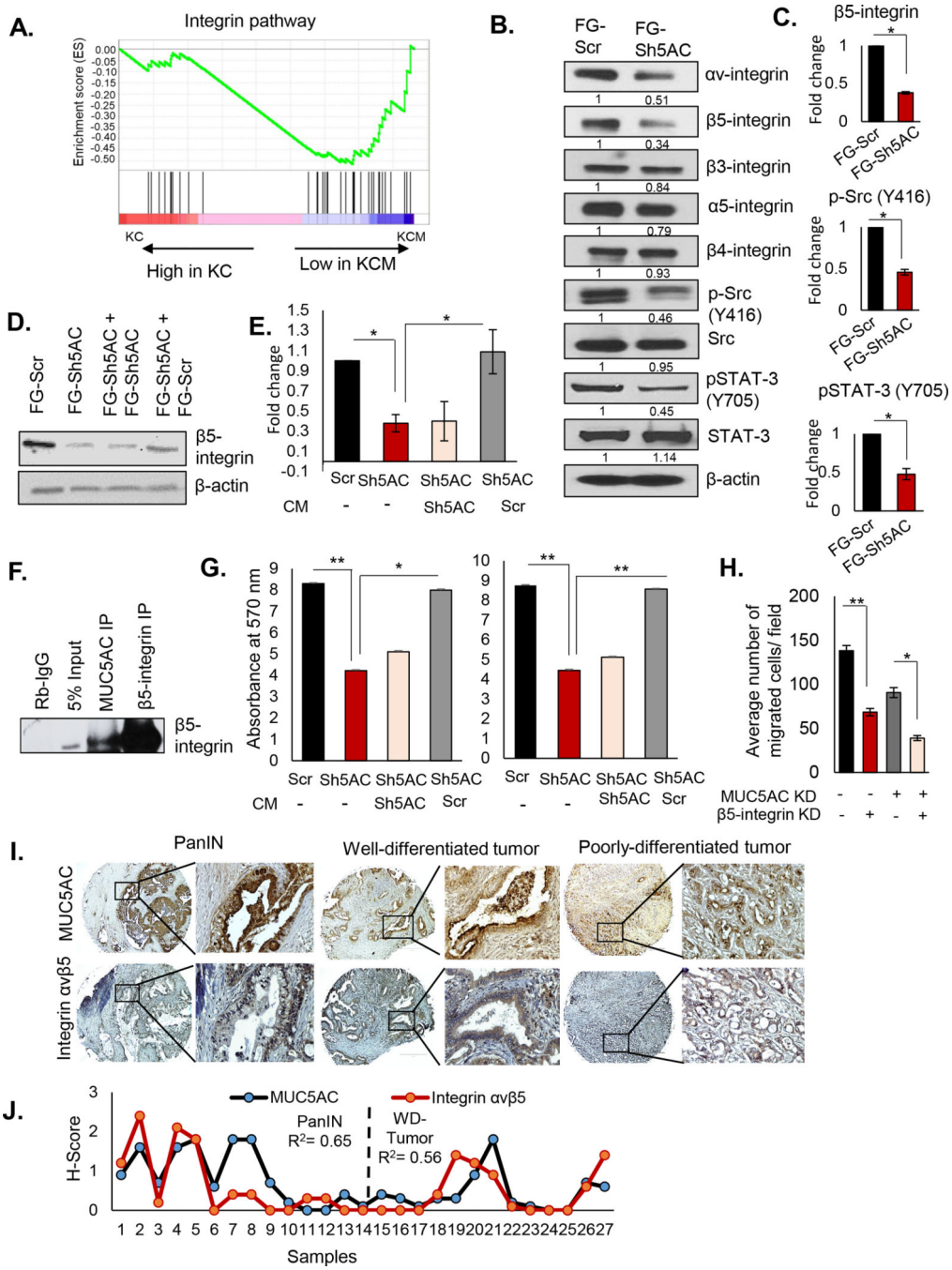

Figure 5: Depletion of MUC5AC disrupts integrin-β5 signaling:

(A) GSEA analysis performed on the RNA-seq. analysis from KC and KCM pancreatic tissues showing downregulation of genes involved in integrin signaling in KCM mice. **(B)** Immunoblot analysis showing reduced expression of integrins αv and β5 upon MUC5AC knockdown in FG/COLO357 cells. Further, MUC5AC knockdown decreased phosphorylation of both tyrosine 416 (Y416) in Src and tyrosine 705 in STAT3 (Y705). Relative fold change of expression of each protein (compared with respect to the control group) is mentioned under each blot (β-actin was used as a loading control for

normalization). **(C)** Quantitative analysis from 3 independent experiments demonstrating a significant reduction in the expression of β5 integrin, pSrc (Y416), and pSTAT3 (Y705) in FG-Sh5AC cells. **(D)** Representative immunoblot and **(E)** Quantitative analysis (n=3) demonstrates that the treatment with supernatant from FG-Scr cells for 48 hours rescues expression of integrin β5 in FG-Sh5AC cells. **(F)** Immunoblot showing the co-immunoprecipitation of integrin-β5 with MUC5AC from FG-COLO357 cells grown on fibronectin-coated plates. The input of 5% cell lysate demonstrates the endogenous expression of integrin-β5 in FG-COLO357 cells. Pulldown with isotype control mouse monoclonal antibody serves as the negative control. **(G)** Quantitative analysis of colorimetric assay reveals that MUC5AC-KD (FG-Sh5AC) cells proliferate significantly better on vitronectin- and fibronectin-coated plates upon 48 hours of treatment with conditioned media from FG-Scr cells as compared to the untreated FG-Sh5AC group, while those treated with conditioned media from FG-Sh5AC cells did not show enhanced proliferation. **(H)** Quantitative representation of the trans-well migration assay demonstrates that MUC5AC-expressing cells with integrin β5-KD lose their migratory potential as compared to the FG-Scr cells bearing functional integrin β5. Knocking down integrin β5 had a marginal effect on the migration of MUC5AC-KD cells compared to the FG-Scr group. **(I)** Immunohistochemical analysis of human PC tissue arrays stained for integrin αvβ5 and MUC5AC along the spectrum of disease progression, viz. PanIN lesions, well-differentiated (WD), and poorly differentiated tumors. Scale bar, 200 uM, adjacent magnified images, 100 uM. **(J)** A statistical analysis demonstrating a significant correlation of integrin αvβ5 and MUC5AC expression in the PanIN lesions (R^2=0.65) and the WD tumors (R^2=0.56) of human PC tissue array.

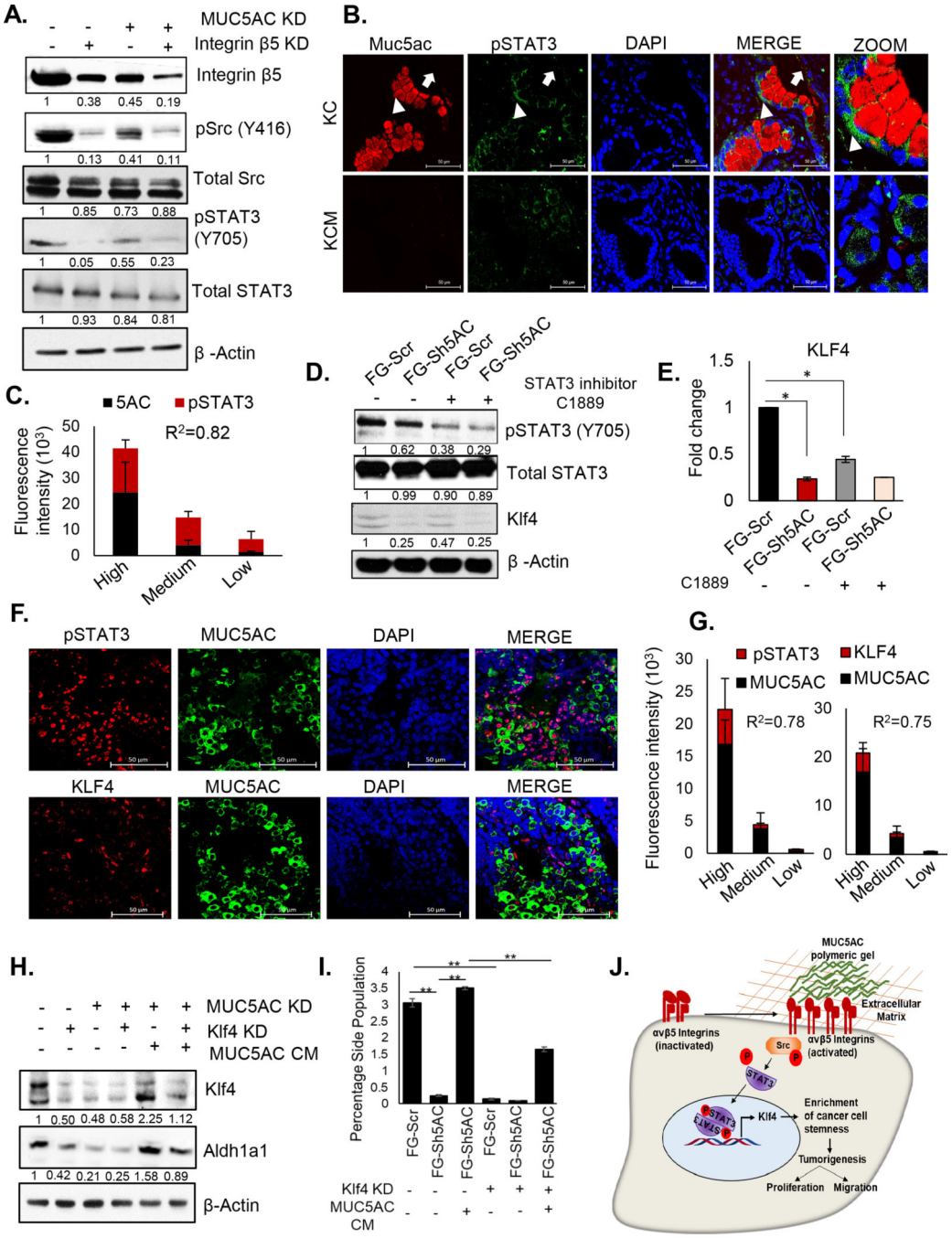

Figure 6: Abrogation of integrin β5/pSrc/pSTAT3 signaling decreases KLF-mediated PC stemness

(A) Immunoblot showing a reduction in the expression of integrins β5, pSrc (Tyr 416), and pSTAT3 (Tyr 705) in FG-Scr cells upon transient KD of integrin β5. This downregulation was much greater in the MUC5AC-expressing cells than in the KD cells (compare lanes 1 and 2 versus lanes 3 and 4). Relative fold change of expression of each protein (compared with respect to the control group) is mentioned under each blot (β-actin was used as a loading control for normalization). **(B)** Representative image and **(C)** Quantitative

illustration of immunofluorescence analysis demonstrates overall less pSTAT3 in KCM and strong positive correlation of MUC5AC and pSTAT3 (R^2 = 0.82) in the PanIN lesions of KC mouse (n=3–5 fields/ tissue, three animals). The co-expression of Muc5ac and pSTAT3 (Y705) in the ductal epithelial cells of KC are shown with white arrowhead and decreased pSTAT3 in cells devoid of Muc5ac are shown with white arrow. **(D)** Representative immunoblot and **(E)** Quantitative analysis (n=3 independent experiments) shows a significant decrease in pSTAT3 and Klf4 expression in the FG-Scr and FG-Sh5AC cells upon treatment with C1889 (p-STAT3 inhibitor). **(F)** Representative images and **(G)** Quantitative illustration of immunofluorescence analysis demonstrated a significant correlation of MUC5AC with pSTAT3 (R^2 = 0.78) and Klf4 (R^2 = 0.75) in the orthotopic tumors (n=3–5 fields/ tissue, 3 animals) from FG/COLO357 cells. **(H)** Immunoblot showing a decrease in Klf4 and Aldh1a1 in FG-Scr and FG-Sh5AC cells upon Klf4-KD. There was a significant increase in Klf4 and Aldh1a1 in FG-Sh5AC cells upon treatment with conditioned media from FG-Scr cells for 48 hours (compare lane 3 to lane 5) which decreased upon Klf4-KD (compare lane 5 to lane 6). Relative fold change of expression of each protein (compared with respect to the control group) is mentioned under each blot (β-actin was used as a loading control for normalization). **(I)** Quantitative representation of percentage side population (SP) demonstrating a significant decrease in SP upon Klf4-KD in MUC5AC expressing cells. There was a drastic increase in SP in the FG-Sh5AC cells upon treatment with condition media from FG-Scr cells and a significant decrease in the same upon Klf4-KD. **(J)** Schematic diagram representing the oncogenic role of MUC5AC during PC progression. Upon Kras-induced overexpression of gel-forming mucin, MUC5AC on the neoplastic cell surface, integrin αvβ5 activates oncogenic signals via pSrc (Y416) and pSTAT3 (Y705). Phosphorylation, dimerization, and nuclear localization of STAT3 lead to the upregulation of Klf4, which in turn, enriches the self-renewing CSCs and thereby promotes tumorigenicity of neoplastic cells. Hence, the depletion of Muc5ac in the murine model delays the metaplastic onset and disease progression.